Photonic crystal-driven spectral concentration for upconversion photovoltaics

Marques-Hueso, Jose; Peretti, Romain; Abargues, Rafael; Richards, Bryce S.; Seassal, Christian; Martínez-pastor, Juan P.

Published in:
Advanced Optical Materials

DOI:
10.1002/adom.201400402

Publication date:
2015

Photonic Crystal-Driven Spectral Concentration for Upconversion Photovoltaics

Jose Marques-Hueso, Romain Peretti, Rafael Abargues, Bryce S. Richards, Christian Seassal, and Juan P. Martínez-Pastor*

The main challenge for applying upconversion (UC) to silicon photovoltaics is the limited amount of solar energy harvested directly via erbium-based upconverter materials (24.5 W m^{-2}). This could be increased up to 87.7 W m^{-2} via spectral concentration. Due to the nonlinear behavior of UC, this could increase the best UC emission by a factor 13. In this paper, the combined use of quantum dots (QDs)—for luminescent down-shifting—and photonic crystals (PCs)—for reshaping the emission—to achieve spectral concentration is shown. This implies dealing with the coupling of colloidal QDs and PC at the high-density regime, where the modes are shifted and broadened. In the first fabricated all-optical devices, the spectral concentration rises by 67%, the QD emission that matches the absorption of erbium-based upconverters increases by 158%, and the vertical emission experiences a 680% enhancement. Remarkably, the PC redshifts the overall emission of the QDs, which could be used to develop systems with low reabsorption losses. In light of this, spectral concentration should be regarded as one of the main strategies for UC photovoltaics.

1. Introduction

Upconversion (UC) represents a growing field due to its multitude of promising applications.[1–3] Different solar cell technologies stand to benefit greatly from UC.[2,4] Despite being by far the leading technology in photovoltaics, the band gap of silicon only allows effective harvesting of light with wavelengths shorter than 1100 nm. Longer wavelengths are lost by transmission, which is one of the main contributors to the Shockley–Queisser limit[5] (30% for silicon devices under one-sun illumination). Via UC, these low-energy photons are harvested by an upconverter that re-emits high-energy photons that are then absorbed by the overlying bifacial silicon solar cell.[2] Following this approach, it has been theoretically calculated that the efficiency limit can rise to 37.4%.[6]

Although several UC approaches exist,[7] UC via lanthanide ions present many advantages, such as stability, easy incorporation into a wide variety of hosts, and a suitable energetic level diagram.[8] Most of the tested materials for near-infrared (NIR) UC are doped with erbium,[9] whose $^4I_{15/2} \rightarrow {}^4I_{13/2}$ broad transition allows absorbance in a 100 nm bandwidth centered around the main peak at about 1523 nm. The absorption of two low-energy (≈1500 nm) photons can then be followed by the emission of one 980 nm upconverted photon (transition $^4I_{11/2} \rightarrow {}^4I_{15/2}$). One of the most studied materials has been $NaYF_4:Er^{3+}$ due to its high UC efficiency, excellent environmental stability, broadband absorption, and low maximum phonon energy that avoids multiphonon relaxation (nonradiative decay).[10] This material has recently provided an additional short-circuit current density due to UC of 4.03 mA cm^{-2} for a silicon cell.[11] Moreover, $NaYF_4$: Er^{3+} can be prepared as bulk or as dispersed nanocrystals,[12] which multiplies the applications of this material, although in nanometric form the UC efficiency decreases by several orders of magnitude.[13]

Furthermore, $NaYF_4:Er^{3+}$ presents an exceptionally wide absorption spectrum from 1470 to 1580 nm due to the different environments of the Er^{3+} ion in this structure.[14] However, this still leaves a large region of the solar spectrum from 1100 to 1470 nm that is unutilized for silicon PV. Other UC materials have been investigated in order to upconvert these unused photons, like Tm^{3+}-doped ceramics that absorb at 1220 nm and emit at 808 nm,[15] and Er^{3+}–Dy^{3+} codoped systems for absorption at 1300 nm.[16] However, in these systems the absorption lines are narrow and the overall conversion efficiency is small. This constraint to absorb narrow bands of the solar spectrum is one of the main limitations[17] of lanthanide-based UC. In the case of nanocrystals, research is being carried out on the use of organic antennas[18] to broaden the absorption range, although it would be difficult to export this technique to bulk materials.

Dr. J. Marques-Hueso
Institute in Signals, Sensors and Systems (ISSS)
Heriot-Watt University
EH14 4AS, Edinburgh, UK
E-mail: J.Marques@hw.ac.uk
Dr. R. Peretti, Dr. C. Seassal
Institut des Nanotechnologies de Lyon (INL)
Université de Lyon
UMR 5270, CNRS, Ecole Centrale de Lyon,
36 Guy de Collongue, F-69134 Ecully Cedex, France
Dr. R. Abargues, Prof. J. P. Martínez-Pastor
UMDO, Instituto de Ciencias de los Materiales
Universidad de Valencia
P.O. Box 22085, 46071, Valencia, Spain
Prof. B. S. Richards
Institute of Microstructure Technology (IMT)
Karlsruhe Institute of Technology
76344, Eggenstein-Leopoldshafen, Germany

DOI: 10.1002/adom.201400402

For these reasons, we hereby propose the use of photonic crystal (PC)-assisted spectral concentration to overcome the transparency losses encountered by silicon UC–PV systems in the 1100–1470 nm range.

2. Spectral Concentration

Figure 1a compares the air mass 1.5 global (AM1.5G) solar irradiance spectrum with the theoretical maximal power density from it that a Si solar cell could convert into electron-hole pairs (gray-shaded area). The absorbance of the $^4I_{15/2} \rightarrow {}^4I_{13/2}$ transition in $NaYF_4:Er^{3+}$ (25%) is depicted in red, and its corresponding UC emission $^4I_{11/2} \rightarrow {}^4I_{15/2}$ at 980 nm, near the band gap of silicon, is shown in blue.

There is a large amount of unutilized photons of the solar spectrum between 1100 and 1350 nm, which could ideally be absorbed by a luminescent species (dye, lanthanide compound, or quantum dot (QD)) and re-emitted[19,20] at the absorption band of the Er^{3+}, which would feed the UC mechanism to obtain greater 980 nm emission. The maximum possible power fraction converted into electron-hole pairs by silicon is 496 W m^{-2}. Due to the electron-hole recombination considered in the Shockley–Queisser limit, this power will be sensibly reduced to produce a current corresponding to a maximum possible power fraction of approximately 300 W m^{-2}. The energy of the solar spectrum that overlaps with the absorption range (1470–1580 nm) of the Er^{3+} upconverter contains 24.5 W m^{-2}. However, a further 78 W m^{-2} can be sourced from the solar spectrum between 1100 and 1350 nm. To downshift these photons to 1523 nm using a luminescent species would incur 19% of nonradiative losses. This means that finally there would be 87.7 W m^{-2} available for UC, which is 3.6 times the usual targeted energy for Er^{3+} UC. Moreover, UC is nonlinear, and the number of emitted photons is proportional to the square of the incident irradiance for a two-photon process.[21] Thus, increasing the incoming irradiance in a real upconverter by a factor 3.6X, would increase the emission up to a factor 13X.

Figure 1b shows the possible schematic implementation of the resulting spectral concentrator investigated here. An UC layer, whose optimal thickness has been calculated[22] to be around 1 mm for $NaYF_4:Er^{3+}$, is placed between the solar cell and the spectral concentrator. The UC is transparent to the photons in the range 1100–1350 nm (③), which are absorbed by the QDs within the spectral concentrator placed behind the UC. The energy level diagram of this last process (③) is shown in Figure 1c. After excitation, the QD relaxes nonradiatively to the exciton state |X>, and finally emits a photon corresponding to this energy. The energy of the incident photon has been reduced slightly via this luminescent down-shifting process, but the emitted photon is now of a suitable wavelength to be absorbed by the UC material. The UC process can follow different paths in the Er^{3+} diagram, but the 980 nm emission peak is dominant, representing 97% of the total emission.[23]

2.1. Absorption by PbSe Quantum Dots

A good candidate for the QD absorber to harvest the unused NIR photons is PbSe. QDs are good absorbers, which offer new opportunities for photovoltaics (PV).[24] PbSe QDs have been studied exhaustively during the last decade due to their tunable NIR optical properties and the easy fabrication.[25] Moreover, photoluminescent quantum yield (PLQY) values in the range of 80% have been reported, thus making it an efficient energy converter.[26] Both Shalav[27] and Strümpel[16] proposed the use of QDs in the NIR for UC PV about a decade ago. An early experiment was performed in 2010, where a device consisting of a

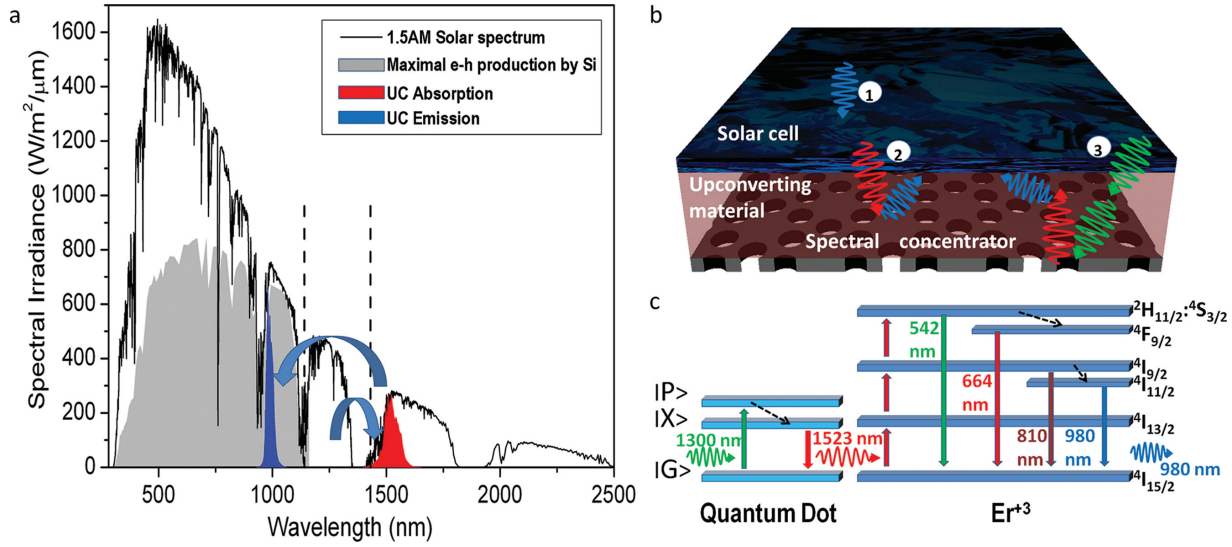

Figure 1. Mechanisms for solar spectral concentration. a) AM1.5G solar spectral irradiance (black line) and highest theoretical electron-hole pair production provided by a silicon solar cell (shadowed area). The red area is the absorbance of $NaYF_4:Er^{3+}$, while the blue area is the main peak of the emission of the upconverter. b) Possible scheme of a silicon solar cell with UC and the photonic crystal spectral concentrator with embedded QDs. Short-wavelength photons are directly absorbed by the Si (①), or after direct UC (②), or by luminescent down-shifting at the spectral concentrator followed by UC (③). c) Mechanism to downshift the energy of an incident photon in the range 1100–1350 nm by a QD, and absorption of its emission by the Er^{3+} ion prior to the UC process.

bifacial solar cell, QDs, and an upconverter was implemented and a small current measured.[20] However, because the wavelength of the excitation source (100 nm broadband LEDs) was able to directly excite the erbium, it wasn't possible to demonstrate the mechanism responsible for the enhancement: the scattering introduced by the QDs and longer path length of the excitation that usually doubles the UC signal[28] or the possible emission of the QDs.

Figure 2 shows the absorption spectrum of PbSe QDs. As can be seen, the absorbance of QDs is typically represented by a broad Gaussian distribution with a width broader than 200 nm, and it redshifts with increasing diameter. This shape adequately matches the AM1.5G solar irradiance spectrum that is represented as the gray-shaded area. From these results, the absorption of a 3.9 nm PbSe QDs suspension would optimally match the maximum of irradiance at 1240 nm and absorb out to the water vapor absorption window that begins at 1350 nm, although other sizes would also be suitable with less efficiency.

However, the emission of the colloidal QDs presents a broad distribution, typically known to be broader than 200 nm,[26,29,30] as can be seen in Figure 2 for 4.7 nm QDs with 214 nm full width at half maximum (FWHM) emission, while the absorption of the UC $NaYF_4:Er^{3+}$ has a bandwidth of only 110 nm. This mismatch results in a large fraction of the light emitted by the QDs being out of range to be absorbed by the UC. Moreover, the shift of the emission with respect to the absorption for PbSe QDs is small (around 100 nm),[26] meaning that the Stokes shift would not be large enough to bridge the available solar radiation and the absorption of the upconverter. Finally, the intersection of absorption and emission in QDs is large, and self-absorption processes can become a problem as with the luminescent solar concentrator technology.[31] For these three reasons, the simple addition of QDs could not significantly enhance the action of the upconverter when using the solar spectrum.[20] Therefore, to solve these challenges, we introduce the use of PCs to tailor the emission of the embedded QDs to suit the Er^{3+} UC absorption.

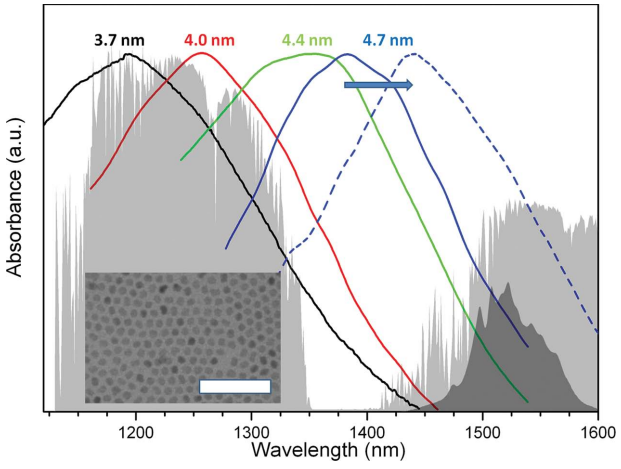

Figure 2. Excitonic absorbance of the synthesised PbSe quantum dots with different sizes (continuous lines). The dashed blue line is the PL of the 4.7 nm QDs. The light gray-shaded area corresponds to the AM1.5G solar spectrum, and the dark grey is the absorbance of $NaYF_4:Er^{3+}$. The inset shows a TEM image of the 4.7 nm QDs (TEM scale bar = 50 nm).

2.2. Emission Modification by Photonic Crystals

The coupling of QDs and PC has attracted huge interest in recent years, especially in the case of epitaxially grown QDs. By changing the density of states, it has been possible to enhance the emission even to induce stimulated emission; firstly by using defective states,[32] and later through the use of low group velocity band-edge modes,[33] where the emission area is extended along the whole PC. In this paper, the latter approach has been pursued using the graphite structure due to its suitable band diagram. This structure has already been used to demonstrate enhanced vertical emission from quantum wells[34] and epitaxial QDs.[35]

Figure 3a shows the band diagram of the InP graphite structure calculated by finite-difference time-domain (FDTD). The distance between neighboring holes (a) is 447 nm, the thickness of the slab 150 nm, and radius (R) 141 nm. The red arrow marks the intersection of two modes with the gamma direction Γ (vertical direction), with resonant wavelengths located at 1530 and 1503 nm. As can be seen, the band is very flat, which indicates that the group velocity of a wave at that frequency propagating within the plane would be very low, and would hence present a tendency to be emitted vertically.

Figure 3b shows the simulated emission from embedded dipoles for different hole radius of the PCs. A larger hole diameter results in a shift of the resonances to higher frequencies. The spatial distribution of the electric field intensity of the modes is depicted at the lower side of the figure. In order to tune the resonance frequency, a series of PC has been fabricated with increasing hole diameter, and their resonance wavelength experimentally determined by measuring their vertical reflectance (Figures 3c and S1, Supporting Information). This provides a set of samples with resonant wavelengths along the range 1490–1550 nm, which coincides well with the maximum of absorption of the $NaYF_4:Er^{3+}$ upconverter.

Next, we have deposited 4.4 nm PbSe QDs on the surface of the sample. This size has been chosen as a compromise between optimum absorption and optimum emission range. The deposition is expected to have two effects. Firstly, the addition of material on the surfaces of the PC results in a decrease in the original radius of the holes, which should redshift the resonant wavelengths. Secondly, the roughening of the surfaces decreases the Q factor[36] of the PC, thus allowing its interaction with a wider range of frequencies.

Figure 4a shows the emission recorded from the QDs on the R = 149–159 nm devices (see Figure S2 (Supporting Information) for more complete measurements). The emission of the QDs on the surface of a nonpatterned area (R = 0 nm) shows a 170 nm FWHM Gaussian emission peak centered at 1386 nm, a region where it is possible to distinguish the water absorption peaks due to the optical beam being propagated through the air before reaching the detector.

Overall, three effects of the PC on the emission of the QDs can be identified. Firstly, the modification in emission spectrum shape is observed. When measuring the emission of the QDs embedded in the PC with a radius of 149 nm, the spectrum changes dramatically and now exhibits a large emission enhancement at 1425 nm (this is more pronounced in Figure 4b, where the PC emission has been normalized by the

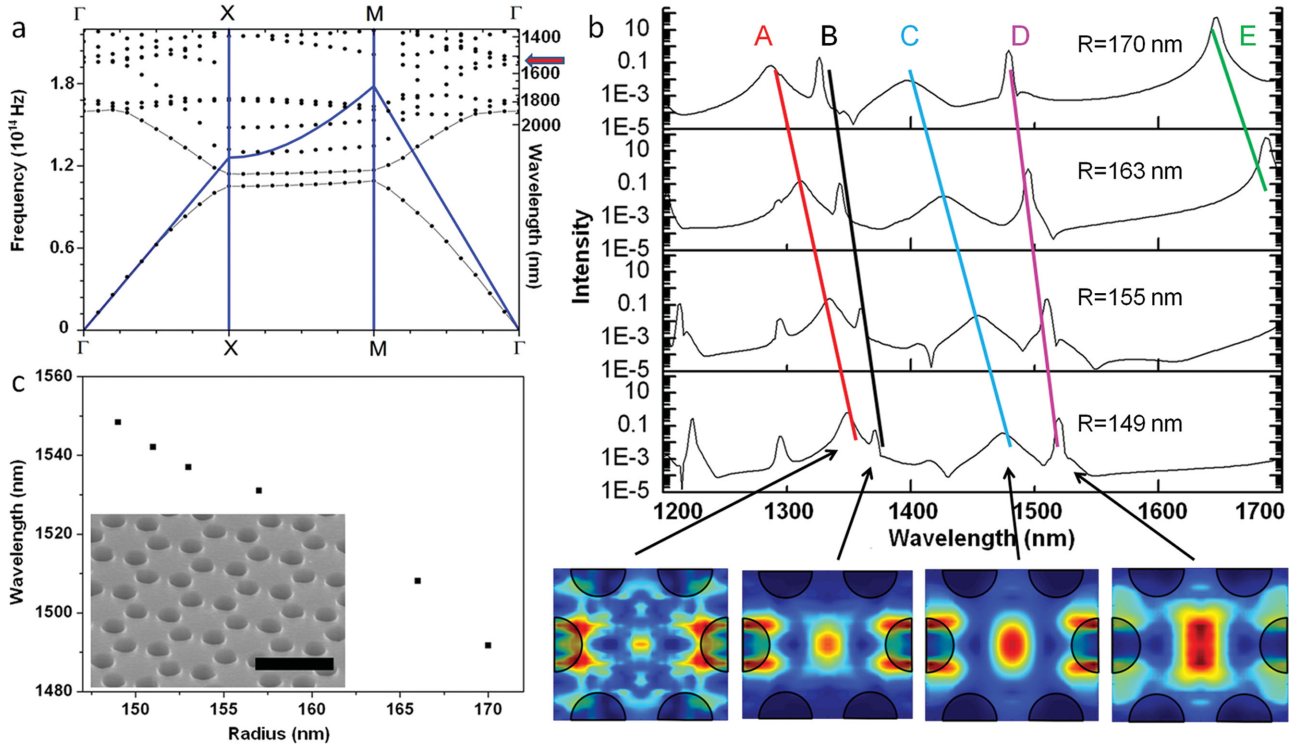

Figure 3. Photonic crystal properties. a) Band diagram of the InP graphite lattice PC ($r = 141$ nm, $a = 447$ nm). The red arrow shows the intersection of the fourth TM band with the vertical direction (Γ). b) Calculated spectral intensity inside the PC membrane showing the displacement of the different modes (labeled as A–E) when the radius increases and corresponding field intensity of some remarkable modes. c) Position of the D mode as measured by reflectivity; Insert: SEM image of one of the fabricated PCs (SEM scale bar = 1 μm).

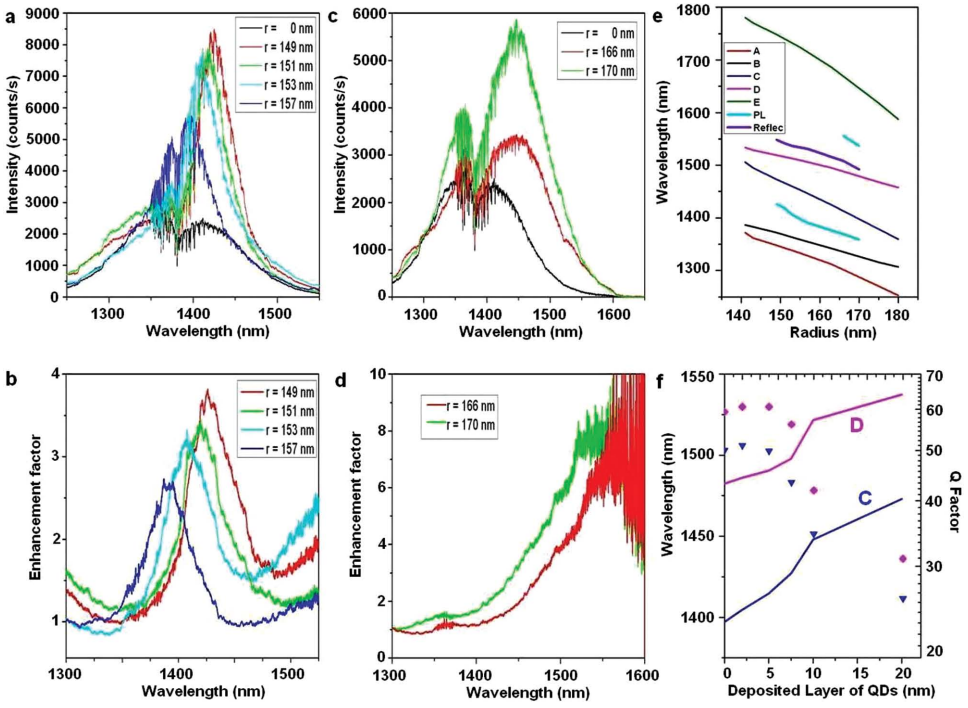

Figure 4. Photoluminescence of the QDs inside the PCs under 810 nm excitation and at 77 K in vacuum. a) Devices with radius 149–157 nm, b) correspondent enhancement factor, c) emission in the PCs with radius 166–170 nm, d) correspondent enhancement factor (notice the different scale from b), e) comparison between the position of the modes (A–E) via simulations and experimental data (reflectivity in purple and PL of the two different peaks in clear blue), and f) simulation of the wavelength (solid line) redshift of the modes C and D and decrease of the Q factors (points) when the layer thickness of deposited QDs increases.

emission in an unpatterned area). The FWHM of the new emission peak is 57 nm, which is of the same order of broadening as has been observed for colloidal QDs on the surface of a PC.[36] Despite the fact that the bandwidth of the mode of the original PC can be extremely narrow (see Figure S1, Supporting Information), the QDs that experience a modification of their emission belong to a wide range of frequencies.[36] This is due to the fact that the colloidal QDs distributed on the surfaces of the PCs introduce asymmetry that results in the broadening of the mode.[37] Due to the fact that the resonances are expected to redshift after the coating, this enhancement should be due to the mode B, because all losses of the mode A correspond to light emission into the substrate while the experimental collection is done from the top (see Figure S3, Supporting Information). The previously measured dipole mode D is expected to be located at longer wavelengths once the QDs are deposited and thus it exceeds the range of measurement.

In addition to the spectral concentration, the shape change of the emission of the QDs embedded in the PC has a second implication. The total emission of the ensemble of QDs in all the devices is redshifted with regard to the emission of QDs outside the PC. This means that the Stokes shift of the QDs can be increased, which is useful for matching the absorbance of the upconverter and reducing self-absorption losses.

For much larger radius of the holes (see Figure 4c,d), a new enhancement peak located at larger wavelengths is observed that is attributed to the presence of the redshifted mode D in the measurement range. Although its intensity is very weak, it is also still possible to see mode B located around 1360 nm. Figure 4e shows the calculated location of the bare structure modes (A–E) via simulations and the position of the D mode as measured by reflectance (purple line). The values for the position of this mode agree with a tolerance of 25 nm. This small deviation (2%) could be due to the inaccuracy measuring the hole dimensions. The wavelengths of the experimental PL peaks of the QDs inside the PCs once normalized by the QDs emission outside the PCs are also represented (light blue). These peaks are shifted with respect to the reflectance and the simulations for the bare PCs, while they follow the same evolution with increasing radius. In order to demonstrate that the deposition of QDs redshifts the resonances, additional FDTD simulations for the R = 170 nm device have been done with increasing QD layer thickness (Figure 4f). These simulations not only show that a thin layer of deposited QDs redshifts the modes, but also that the Q factor decreases, thus explaining the observed broadening of the PL respect to the bare structure.

The third and last effect identified is that the vertical emission of the QDs is also increased at some wavelengths by the PCs, as expected.[37] Although it cannot be guaranteed that the amount of QDs on each device is exactly the same and this is acknowledged to be a source of inaccuracy, Figure 4b shows a consistent tendency of the peaks that reveals a maximum enhancement factor of the vertical emission of a factor 2.6–3.8 depending on the sample. In the case of the mode observed at higher hole sizes (Figure 4d), the enhancement represents a factor 6.4–7.8. This is consistent with literature, which corroborates that mode D is the most efficient for light extraction.[34]

In order to quantify the spectral concentration, we have defined as a figure-of-merit for each device the percentage of the emission that occurs within a 50 nm window around the main peak. This value has been chosen for being approximately the width of the narrowest Gaussian peak, and the calculated results can be seen in **Table 1**. While the most intense 50 nm range at the unpatterned area only represents 25.8% of the total emission, inside the R = 149 nm PC this concentration increases to 43% of the total. This means that the spectral concentration increases by 66%.

The results are similar for all the devices with small radius (149–157 nm, Figure 4a,b). For the devices with a large radius (166–170 nm, Figure 4c,d) it is possible to see that the intensity of the brightest 50 nm range represents a similar value to the unpatterned case. This is due to the fact that in these devices the active mode is a different one much far away from the center of the Gaussian of the natural emission. Table 1 also shows the overlap of the emission with the absorption of the UC material $NaYF_4:Er^{3+}$ and the largest enhancement factor and their wavelengths. In the most remarkable case (R = 170 nm), the QD emission that matches the absorption of the upconverter increases by 158%.

2.3. Considerations for Implementation for Solar Energy Harvesting

Finally, we have evaluated the magnitude of the absorbance of PbSe QDs in order to gain an insight into the recommended size for solar absorption (see Figure S4, Supporting Information). The extinction coefficient of the PbSe QDs is calculated to be 0.0915 L g^{-1} cm^{-1} at the peak that corresponds to the ground state excitonic absorption. This leads to an absorption coefficient for the PbSe QDs of $\alpha = 0.864$ cm^{-1} for a concentration of 9.44 g L^{-1}, in line with the relevant literature.[29]

With this value, in order to absorb 50% of the intensity of the incoming light at the maximum, a 5.4 μm thick layer of close-packed QDs would be required. Although this thickness is rela-

Table 1. Photoluminescence of the PbSe QDs outside (R = 0 nm) and inside the different PCs.

Hole radius of PC [nm]	0	149	151	153	157	166	170
Percentage within 50 nm window [%]	25.8	43.0	40.8	42.1	39.4	25.6	29.4
Central wavelength of 50 nm window [nm]	1383	1425	1419	1410	1395	1444	1448
Overlap with $NaYF_4:Er^{3+}$ absorption (1470–1580) [%]	9.7	9.3	7.2	11.5	8.0	24.7	25.0
Wavelength of the largest enhancement factor	N.A.	1426	1419	1406	1390	1556	1537
Largest enhancement factor	N.A.	3.8	3.4	3.2	2.6	6.4	7.8

tively large, two things can be done to overcome this problem in the future. Firstly, in the same way that we have demonstrated emission assisted by the PC, it would be possible to assist the absorption of light by coupling the incident illumination to a different mode of the PC,[37] which would dramatically reduce the required thickness of the device.[38] Secondly, other fabrication techniques could be used to produce such deep structures, or 3D PCs. Among them, we can find two-photon polymerization,[39] direct laser writing,[40] 3D colloidal crystals,[41] photonic fibers pulling,[42] and anodic etching.[43] Finally, core/shell QDs could be used due to the possibility of tuning the Stokes shift by modifying the geometry of the QDs,[44] while also benefitting from increased PLQY and environmental stability.

3. Conclusion

In summary, we have shown the use of NIR QDs and PCs for achieving spectral concentration and vertical emission enhancement at the desired wavelength range. Via such an approach, a portion of the solar energy in the 1100–1470 nm range could be redshifted to match the absorption band of the most common Er^{3+}-doped upconverters (1470–1580 nm). The effect of the PC modifies three aspects of the emission of the QDs: i) it achieves spectral concentration by narrowing the emission band, ii) it increases the Stokes shift of the QDs, and iii) it increases the vertical emission. The first results exposed here show that the spectral concentration has been increased by 67%, the emission of the QDs that matches the absorption range of the upconverter has been increased by 158%, and finally the emission in the vertical direction has experienced the largest enhancement by a factor of 7.8 times. In light of these results, spectral concentration should be regarded as one of the strategies to enhance UC for PV, in the same way as other strategies currently under study, such as the use of plasmonic resonances,[45,46] PCs,[47] or postcell concentration.[48]

4. Experimental Section

The simulations have been done using RSOFT full-wave FDTD software, using periodic boundary condition for lateral (*X* and *Y*) axis and perfectly matched layer condition for vertical axis. The size of the calculation mesh was about 20 nm (round in order to have an integral number of calculation cells in a PC cell in all directions). We used broadband sources for the spectral simulation and a continuous one for spatial distribution of field of the modes. Q factor analyses were performed using harmonic inversion software Harminv. The layer of QDs has been simulated assuming an equivalent layer of 27% PbSe and 73% oleate shell on all the surfaces of the PC.

The PbSe QDs were synthesized by heating a mixture of PbO (4.00 mmol), oleic acid (10.00 mmol), and 1-octadecene (Aldrich) at 150 °C. Then, a solution of selenium (8.00 mmol) in trioctylphosphine was swiftly injected into this hot solution, and the reaction mixture was allowed to cool to 130 °C to obtain different-sized QDs by controlling the reaction time.[25] The QDs were purified by successive precipitation with acetone, centrifugation, and redispersion in chloroform. Once purified three times, PbSe QDs were redispersed in tetrachloroethylene. The concentration has been determined by drying and direct weighting. The absorbance of the QDs has been measured at room temperature using a spectrometer (Perkin Elmer 950) with an integrating sphere and a quartz cuvette with a path length of 2 mm.

The PCs have been fabricated on a 150 nm InP film on glass created by wafer bonding.[49] 100 nm of SiO_2 has been sputtered on top. The pattern is generated by electron-beam lithography at 30 KV using PMMA as a resist, and using a small increment of the dose between neighboring devices to increase the hole size in small amounts. The PCs area is 30×30 μm^2 and the distance between them is 100 μm. The pattern is transferred to the SiO_2 layer by reactive ion etching (RIE) using CHF_3 at 15 mTorr, 16 sccm, and 100 W. The remaining PMMA is removed by O_2 plasma (20 sccm, 100 mTorr, 100 W). The InP layer is then patterned by a CH_4/H_2 plasma (15/30 sccm, 30 mTorr, 200 W). The remaining SiO_2 is finally removed by RIE. The deposition of the QDs has been done by drop casting at room temperature.

The photoluminescence of the deposited QDs has been measured using a homemade confocal microscope. An 810 nm laser is focused on the samples that are placed at a cryostat at 77 K. The same objective (NA = 0.9) is used to collect the emitted signal and the light is guided by optical fiber to a monochromator and InGaAs CCD detector (iDus InGaAs 492–1.7, Andor Technology). The low temperature provides a stronger signal for measurement and the involved vacuum prevents further oxidation,[29,50] which is known to quench the emission, without modifying the effect of the PC (the photoluminescence peak at 77 K is only redshifted about 50 nm in respect to the room temperature for this size of QD.[30]

The reflectivity of the PCs has been measured by focusing the light of a halogen lamp on the samples via an optical fiber. The reflectance in the normal direction is recorded by a fiber that guides the signal to an optical spectrum analyzer.

Supporting Information

Supporting Information is available from the Wiley Online Library or from the author.

Acknowledgements

The authors acknowledge Stewart Burt for the artwork, and Josep Canet, from the University of Valencia, for his assistance with the equipment for photoluminescence, as well as the funding from the Engineering and Physical Sciences Research Council (EPSRC) project "Luminescent Lanthanide Layers for Enhanced Photovoltaic Performance (LEAP)" (EP/I013245/1), the European Community's Seventh Framework Program (FP7/2007–2013) under grant agreement no. [246200], the Generalitat Valenciana and Spanish MINECO under Grants PROMETEOII/2014/059 and TEC2011-29120-C05-01.

Received: September 9, 2014
Revised: November 5, 2014
Published online: December 2, 2014

[1] a) M. Haase, H. Schäfer, *Angew. Chem Int. Ed.* **2011**, *50*, 5808; b) N. M. Idris, M. K. Gnanasammandhan, J. Zhang, P. C. Ho, R. Mahendran, Y. Zhang, *Nat. Med.* **2012**, *18*, 1580; c) C. Zhang, H.-P. Zhou, L.-Y. Liao, W. Feng, W. Sun, Z.-X. Li, C.-H. Xu, C.-J. Fang, L.-D. Sun, Y.-W. Zhang, C.-H. Yan, *Adv. Mater.* **2010**, *22*, 633; d) B. Dong, B. Cao, Y. He, Z. Liu, Z. Li, Z. Feng, *Adv. Mater.* **2012**, *24*, 1987.

[2] A. Shalav, B. S. Richards, T. Trupke, K. W. Krämer, H. U. Güdel, *Appl. Phys. Lett.* **2005**, *86*, 013505.

[3] A. Mukherjee, *Appl. Phys. Lett.* **1993**, *62*, 3423.

[4] a) L. T. Su, S. K. Karuturi, J. Luo, L. Liu, X. Liu, J. Guo, T. C. Sum, R. Deng, H. J. Fan, X. Liu, A. I. Y. Tok, *Adv. Mater.* **2013**, *25*, 1603; b) J. De Wild, J. K. Rath, A. Meijerink, W. G. J. H. M. Van Sark,

R. E. I. Schropp, *Sol. Energy Mater. Sol. Cells* **2010**, *94*, 2395; c) G.-B. Shan, G. P. Demopoulos, *Adv. Mater.* **2010**, *22*, 4373.
[5] W. Shockley, H. J. Queisser, *J. Appl. Phys.* **1961**, *32*, 510.
[6] T. Trupke, M. Green, P. Wurfel, *J. Appl. Phys.* **2002**, *92*, 4117.
[7] Y. Y. Cheng, B. Fuckel, R. W. MacQueen, T. Khoury, R. G. C. R. Clady, T. F. Schulze, N. J. Ekins-Daukes, M. J. Crossley, B. Stannowski, K. Lips, T. W. Schmidt, *Energy Environ. Sci.* **2012**, *5*, 6953.
[8] a) B. M. van der Ende, L. Aarts, A. Meijerink, *Phys. Chem. Chem. Phys.* **2009**, *11*, 11081; b) X. Huang, S. Han, W. Huang, X. Liu, *Chem. Soc. Rev.* **2013**, *42*, 173.
[9] a) C. Strümpel, M. McCann, G. Beaucarne, V. Arkhipov, A. Slaoui, V. Švrček, C. Del Cañizo, I. Tobias, *Sol. Energy Mater. Sol. Cells* **2007**, *91*, 238; b) A. Shalav, B. S. Richards, M. A. Green, *Sol. Energy Mater. Sol. Cells* **2007**, *91*, 829.
[10] a) K. W. Kramer, D. Biner, G. Frei, H. U. Gudel, M. P. Hehlen, S. R. Luthi, *Chem. Mater.* **2004**, *16*, 1244; b) A. Ivaturi, S. K. MacDougall, R. Martín-Rodríguez, M. Quintanilla, J. Marques-Hueso, K. W. Kramer, A. Meijerink, B. S. Richards, *J. Appl. Phys.* **2013**, *114*, 013505; c) S. K. MacDougall, A. Ivaturi, J. Marques-Hueso, K. W. Krämer, B. S. Richards, *Opt. Express* **2012**, *20*, A879; d) S. K. W. MacDougall, A. Ivaturi, J. Marques-Hueso, K. W. Krämer, B. S. Richards, *Sol. Energy Mater. Sol. Cells* **2014**, *128*, 18.
[11] S. Fischer, B. Fröhlich, H. Steinkemper, K. W. Krämer, J. C. Goldschmidt, *Sol. Energy Mater. Sol. Cells* **2014**, *122*, 197.
[12] S. Heer, K. Kömpe, H. U. Güdel, M. Haase, *Adv. Mater.* **2004**, *16*, 2102.
[13] J.-C. Boyer, F. C. J. M. van Veggel, *Nanoscale* **2010**, *2*, 1417.
[14] C. Renero-Lecuna, R. Martín-Rodríguez, R. Valiente, J. González, F. Rodríguez, K. W. Krämer, H. U. Güdel, *Chem. Mater.* **2011**, *23*, 3442.
[15] H. Lin, J. Marqués-Hueso, D. Chen, Y. Wang, B. S. Richards, *Mater. Res. Bull.* **2012**, *47*, 4433.
[16] C. Strümpel, M. McCann, C. del Cañizo, I. Tobias, P. Fath, presented at 20th EPVSEC, Barcelona, Spain **2005**.
[17] J. A. Briggs, A. C. Atre, J. A. Dionne, *J. Appl. Phys.* **2013**, *113*124509.
[18] W. Zou, C. Visser, J. A. Maduro, M. S. Pshenichnikov, J. C. Hummelen, *Nat. Photonics* **2012**, *6*, 560.
[19] J. C. Goldschmidt, P. Loper, S. Fischer, S. Janz, M. Peters, S. W. Glunz, G. Willeke, E. Lifshitz, K. Kramer, D. Biner, presented at Optoelectronic and Microelectronic Materials and Devices (COMMAD), Sydney, **2008**.
[20] A. C. Pan, C. del Cañizo, E. Cánovas, N. M. Santos, J. P. Leitão, A. Luque, *Sol. Energy Mater. Sol. Cells* **2010**, *94*, 1923.
[21] M. Pollnau, D. Gamelin, S. Lüthi, H. Güdel, M. Hehlen, *Phys. Rev. B* **2000**, *61*, 3337.
[22] A. Boccolini, J. Marques-Hueso, B. S. Richards, *Opt. Lett.* **2014**, *39*, 2904.
[23] J. F. Suyver, A. Aebischer, D. Biner, P. Gerner, J. Grimm, S. Heer, K. W. Krämer, C. Reinhard, H. U. Güdel, *Opt. Mater.* **2005**, *27*, 1111.
[24] A. K. Rath, M. Bernechea, L. Martinez, F. P. G. de Arquer, J. Osmond, G. Konstantatos, *Nat. Photonics* **2012**, *6*, 529.
[25] W. W. Yu, J. C. Falkner, B. S. Shih, V. L. Colvin, *Chem. Mater.* **2004**, *16*, 3318.
[26] H. Du, C. Chen, R. Krishnan, T. D. Krauss, J. M. Harbold, F. W. Wise, M. G. Thomas, J. Silcox, *Nano Lett.* **2002**, *2*, 1321.
[27] A. Shalav, *Ph.D. Thesis*, University of New South Wales, Sydney **2006**.
[28] T. F. Schulze, Y. Y. Cheng, B. Fückel, R. W. MacQueen, A. Danos, N. J. L. K. Davis, M. J. Y. Tayebjee, T. Khoury, R. G. C. R. Clady, N. J. Ekins-Daukes, M. J. Crossley, B. Stannowski, K. Lips, T. W. Schmidt, *Aust. J. Chem.* **2012**, *65*, 480.
[29] Q. Dai, Y. Wang, X. Li, Y. Zhang, D. J. Pellegrino, M. Zhao, B. Zou, J. Seo, Y. Wang, W. W. Yu, *ACS Nano* **2009**, *3*, 1518.
[30] E. Pedrueza, A. Segura, R. Abargues, J. Bosch Bailach, J. C. Chervin, J. P. Martínez-Pastor, *Nanotechnology* **2013**, *24*, 205701.
[31] a) L. R. Wilson, B. C. Rowan, N. Robertson, O. Moudam, A. C. Jones, B. S. Richards, *Appl. Opt.* **2010**, *49*, 1651; b) A. Boccolini, J. Marques-Hueso, D. Chen, Y. Wang, B. S. Richards, *Sol. Energy Mater. Sol. Cells* **2014**, *122*, 8.
[32] O. Painter, R. K. Lee, A. Scherer, A. Yariv, J. D. O'Brien, P. D. Dapkus, I. Kim, *Science* **1999**, *284*, 1819.
[33] C. Monat, C. Seassal, X. Letartre, P. Regreny, P. Rojo-Romeo, P. Viktorovitch, M. Le Vassor d'Yerville, D. Cassagne, J. P. Albert, E. Jalaguier, S. Pocas, B. Aspar, *Appl. Phys. Lett.* **2002**, *81*, 5102.
[34] B. Ben Bakir, C. Seassal, X. Letartre, P. Viktorovitch, M. Zussy, L. Di Cioccio, J. M. Fedeli, *Appl. Phys. Lett.* **2006**, *88*, 081113.
[35] B. Ben Bakir, C. Seassal, X. Letartre, P. Regreny, M. Gendry, P. Viktorovitch, M. Zussy, L. Di Cioccio, J.-M. Fedeli, *Opt. Express* **2006**, *14*, 9269.
[36] J. Yang, J. Heo, T. Zhu, J. Xu, J. Topolancik, F. Vollmer, R. Ilic, P. Bhattacharya, *Appl. Phys. Lett.* **2008**, *92*, 261110.
[37] N. Ganesh, W. Zhang, P. C. Mathias, E. Chow, J. A. N. T. Soares, V. Malyarchuk, A. D. Smith, B. T. Cunningham, *Nat. Nano* **2007**, *2*, 515.
[38] a) G. Gomard, R. Peretti, E. Drouard, X. Meng, C. Seassal, *Opt. Express* **2013**, *21*, A515; b) Y. Park, E. Drouard, O. El Daif, X. Letartre, P. Viktorovitch, A. Fave, A. Kaminski, M. Lemiti, C. Seassal, *Opt. Express* **2009**, *17*, 14312.
[39] J. Li, B. Jia, G. Zhou, M. Gu, *Opt. Express* **2006**, *14*, 10740.
[40] M. J. Ventura, M. Gu, *Adv. Mater.* **2008**, *20*, 1329.
[41] a) P. Lodahl, A. Floris van Driel, I. S. Nikolaev, A. Irman, K. Overgaag, D. Vanmaekelbergh, W. L. Vos, *Nature* **2004**, *430*, 654; b) J. Gutmann, H. Zappe, J. C. Goldschmidt, *Phys. Rev. B* **2013**, *88*, 205118.
[42] P. Russell, *Science* **2003**, *299*, 358.
[43] W. Lee, R. Ji, U. Gosele, K. Nielsch, *Nat. Mater.* **2006**, *5*, 741.
[44] B. De Geyter, Y. Justo, I. Moreels, K. Lambert, P. F. Smet, D. Van Thourhout, A. J. Houtepen, D. Grodzinska, C. de Mello Donega, A. Meijerink, D. Vanmaekelbergh, Z. Hens, *ACS Nano* **2010**, *5*, 58.
[45] C. A. Ashwin, G.-E. Aitzol, A. Hadiseh, A. D. Jennifer, *J. Opt.* **2012**, *14*, 024008.
[46] W. Zhang, F. Ding, S. Y. Chou, *Adv. Mater.* **2012**, *24*, OP236.
[47] C. M. Johnson, P. J. Reece, G. J. Conibeer, *Opt. Lett.* **2011**, *36*, 3990.
[48] G. E. Arnaoutakis, J. Marques-Hueso, A. Ivaturi, K. W. Krämer, S. Fischer, J. C. Goldschmidt, B. S. Richards, *Opt. Express* **2014**, *22*, A452.
[49] C. Seassal, C. Monat, J. Mouette, E. Touraille, B. B. Bakir, H. T. Hattori, J. L. Leclercq, X. Letartre, P. Rojo-Romeo, P. Viktorovitch, *IEEE J. Sel. Topics Quantum Electron.* **2005**, *11*, 395.
[50] H. E. Chappell, B. K. Hughes, M. C. Beard, A. J. Nozik, J. C. Johnson, *J. Phys. Chem. Lett.* **2011**, *2*, 889.